ChemPubSoc Europe

DOI: 10.1002/chem.201601142

CHEMISTRY A European Journal Full Paper

Structure–Activity Relationships

Host–Guest Binding-Site-Tunable Self-Assembly of Stimuli-Responsive Supramolecular Polymers

Hao Yao, Miao Qi, Yuyang Liu, and Wei Tian*[a]

Abstract: Despite the remarkable progress made in controllable self-assembly of stimuli-responsive supramolecular polymers (SSPs), a basic issue that has not been consideration to date is the essential binding site. The noncovalent binding sites, which connect the building blocks and endow supramolecular polymers with their ability to respond to stimuli, are expected to strongly affect the self-assembly of SSPs. Herein, the design and synthesis of a dual-stimuli thermo- and photoresponsive Y-shaped supramolecular polymer (SSP2) with two adjacent β-cyclodextrin/azobenzene (β-CD/Azo) binding sites, and another SSP (SSP1) with similar building blocks, but only one β-CD/Azo binding site as a control, are described. Upon gradually increasing the polymer solution temperature or irradiating with UV light, SSP2 self-assemblies with a higher binding-site distribution density; exhibits a flower-like morphology, smaller size, and more stable dynamic aggregation process; and greater controllability for drug-release behavior than those observed with SSP1 self-assemblies. The host–guest binding-site-tunable self-assembly was attributed to the positive cooperativity generated among adjacent binding sites on the surfaces of SSP2 self-assemblies. This work is beneficial for precisely controlling the structural parameters and controlled release function of SSP self-assemblies.

Introduction

Stimuli-responsive supramolecular polymers (SSPs), which can self-assemble into various tunable nanostructures, such as vesicles, micelles, nanoparticles, microcapsules, hydrogels, and tubes, have attracted growing interest in the past few decades due to their applications in chemistry, biotechnology, and materials science.[1] Compared with traditional covalent stimuli-responsive polymers (CSPs), SSPs possess specific weak and reversible noncovalent interactions, such as hydrogen bonding,[2] metal–ligand coordination,[3] and host–guest interactions,[4] between the two immiscible blocks. Furthermore, stimuli-responsive properties of SSPs can be inherited from their polymer building blocks and the introduction of noncovalent binding sites, which endows them with more versatile tunable properties and functions.

Precisely controlling the structural parameters and function of SSP self-assemblies is a major topic in the field.[5] According to reports in the literature,[6] the self-assembly behavior of SSPs can be tuned by adjusting polymer (block species and degree of polymerization (DP) of building blocks), solution (solvent species and selective solvent content),[7] and stimulus (e.g., pH, light, temperature, and ultrasound) parameters.[8] Barner-Kowollik et al. reported a series of SSPs with various topologies, such as ABA linear, star, H, and brush.[9] Zhou et al. reported a novel Janus particle and supramolecular block copolymer that could self-assemble into unilamellar bilayer vesicles and disassemble reversibly under UV irradiation.[10] Yuan et al. described a voltage-responsive block copolymer through β-cyclodextrin (β-CD)/ferrocene complexation that could reversibly self-assemble and disassemble in response to voltage changes.[11] Nevertheless, in these systems, supramolecular binding sites located in the backbone of the SSPs only served as scaffolds. From the viewpoint of structure–property relationships, binding sites are the key component of SSPs and should have a pronounced effect on their solution properties. However, to the best of our knowledge, the influence of binding sites on the self-assembly and function of SSPs has not been reported to date.

On the other hand, cooperativity is widespread in enzyme control and many other vital biological processes, and has been rigorously defined in the case of multiple intermolecular bindings of a monovalent ligand to a polyvalent macromolecule.[12] Inspired by cooperativity, we intended to design an SSP containing two adjacent host–guest binding sites on one chain end (Scheme 1 A). In this case, the structural parameters and function of SSP self-assemblies may be subject to regulation on the basis of cooperativity among adjacent host–guest binding sites under external stimuli, such as temperature or light (Scheme 1 A–E).

Based on the above consideration and our recent work on the construction of SSPs,[13] we first designed and synthesized

[a] H. Yao, M. Qi, Prof. Dr. Y. Liu, Prof. Dr. W. Tian
The Key Laboratory of Space Applied Physics and Chemistry
Ministry of Education and Shanxi Key Laboratory
of Macromolecular Science and Technology, School of Science
Northwestern Polytechnical University, Xi'an
710072 (P.R. China)
Fax: (+86) 029-88431619
E-mail: happytw_3000@nwpu.edu.cn

Supporting information for this article is available on the WWW under http://dx.doi.org/10.1002/chem.201601142.

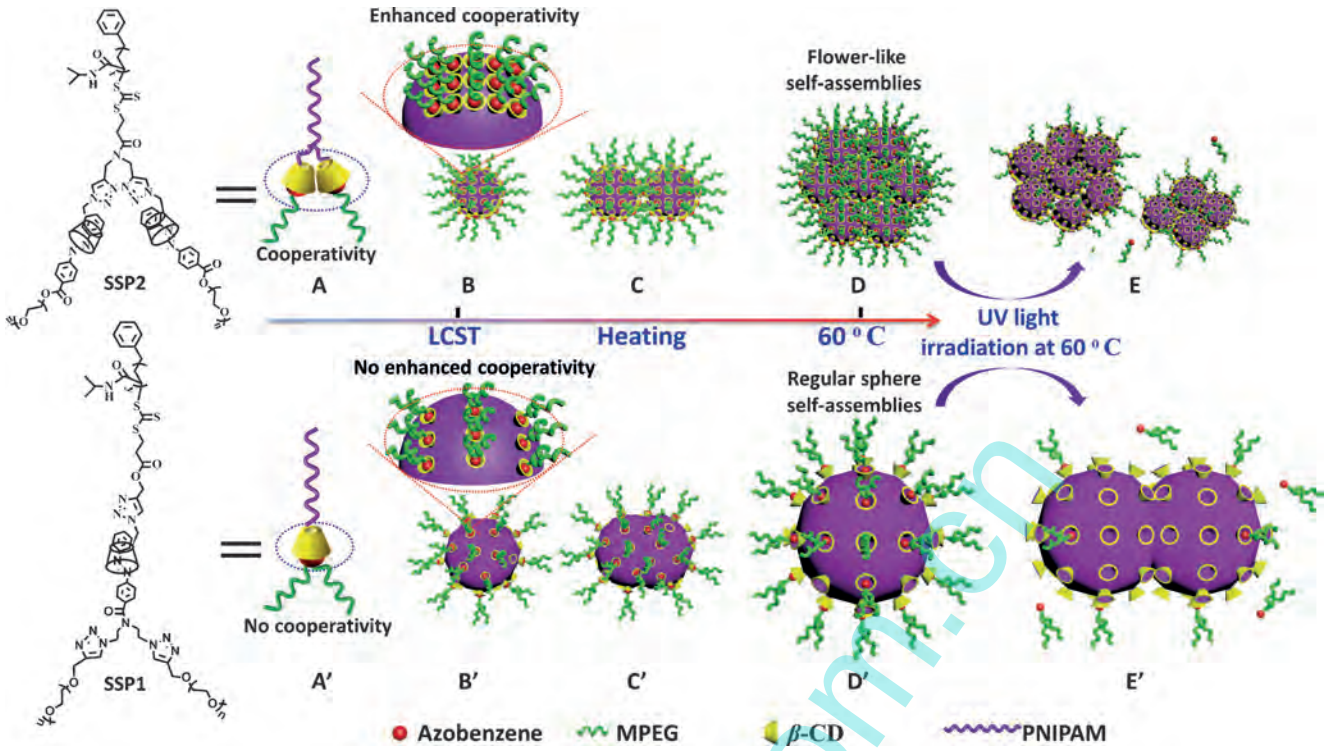

Scheme 1. Representation of the host–guest binding-site-tunable self-assembly mechanism of dual thermo- and photoresponsive supramolecular polymers. Chemical structures of SSP2 (A) and SSP1 (A′) constructed from one and two host–guest interactions, respectively. The positive cooperativity generated by the adjacent β-CD/azobenzene (Azo) binding sites leads to the stronger binding strength of SSP2 than that of SSP1 without cooperativity. When heating the solution above the lower critical solution temperature (LCST), the surfaces of self-assemblies of SSP2 (A, B) have a higher β-CD/Azo binding-site distribution density than those of SSP1 (A′, B′), leading to enhanced cooperativity. During further heating, the enhanced cooperativity of the hydrophilic shell layer of self-assemblies of SSP2 (B, C) plays an important role in steadying the hydrophobic core layer compared with that of SSP1 (B′, C′). The formation of a flower-like morphology with smaller sizes of self-assemblies of SSP2 (C, D) than those of SSP1 (C′, D′) with a regularly spherical structure and bigger size at 60 °C. Through irradiation with UV light at 60 °C, the enhanced cooperativity endows self-assemblies of SSP2 (D, E) with a more stable self-assembly state and avoids coalescence, unlike self-assemblies SSP1 (D′, E′).

the Y-shaped SSP2, which consisted of two adjacent β-CD/Azo host–guest binding sites, one poly(*N*-isopropylacrylamide) (PNIPAM) arm and two methoxypolyethylene glycol (MPEG) arms (Scheme 1 A), as well as another Y-shaped SSP1 containing one such binding site and similar building blocks as a control (Scheme 1 A′). With the introduction of thermoresponsive PNIPAM segments[14] and photosensitive β-CD/Azo complexes,[15] the influence of the binding site on the self-assembly of SSPs can be easily investigated by adjusting the temperature and light irradiation of the solution (Scheme 1 A–E and A′–E′). Compared with SSP1 self-assemblies, SSP2 self-assemblies exhibited a flower-like morphology and smaller size with increasing solution temperature. Meantime, SSP2 self-assemblies presented a much more stable self-assembly process than those of SSP1 self-assemblies when the polymer solutions were heated or irradiated by UV light. Additionally, the drug-release behavior of doxorubicin (DOX) from SSP2 self-assemblies was more controllable than that of SSP1 self-assemblies, regardless of increasing temperature or UV irradiation. Cooperativity between adjacent β-CD/Azo binding sites was proposed as a possible mechanism for the tunable self-assembly process and controlled release function.

Results and Discussion

To obtain the target SSP1 and SSP2 self-assemblies, several building blocks, including singly or doubly β-CD-terminated PNIPAM (PNIPAM-β-CD or PNIPAM-2(β-CD)), as well as Azo-mid or -ended MPEG (Azo-2MPEG and Azo-MPEG), were first synthesized by reversible addition fragmentation chain-transfer polymerization (RAFT) and a click reaction, according to the routes shown in Scheme S1–S4 in the Supporting Information. All polymer precursors were well defined and characterized by ^{1}H and ^{13}C NMR spectroscopy, FTIR spectroscopy, ESI-MS, and size exclusion chromatography/multiangle laser light scattering (SEC-MALLS). The characterization data and corresponding spectra are provided in Figures S1–S25 and Table S1 in the Supporting Information. It should be noted that, although the SEC curves demonstrated tiny lower-molecular-weight shoulders (Figure S15 in the Supporting Information), the molecular weights of these polymers were still well controlled. With the well-defined building blocks, the formation of SSP1 and SSP2 was facilitated by directly dissolving PNIPAM-β-CD and Azo-2MPEG or PNIPAM-2(β-CD) and Azo-MPEG in water in stoichiometric quantities, respectively. Subsequently, 2D NOESY NMR, ^{1}H NMR in D_2O, and UV/Vis absorption spectra were performed

to confirm the formation of host–guest complexes in SSP1 and SSP2.

The 2D NOESY NMR spectra of SSP1 and SSP2 are shown in Figure 1 A and B, respectively. The appearance of intermolecular correlations between the internal H3 and H5 protons ($\delta =$ 3.5–4.0 ppm) in the inner cavity of β-CD and the protons of the Azo group ($\delta = 7.1$–8.2 ppm) indicated the formation of the host–guest complexes in both SSPs. ^{1}H NMR spectra of SSP1 and SSP2 in D_2O are shown in Figure S26 in the Supporting Information. Figure S26a and c in the Supporting Information refers to the Azo protons of Azo-2MPEG and Azo-MPEG (H_a–H_d). The addition of an equimolar amount of PNIPAM-β-CD to Azo-2MPEG and PNIPAM-2(β-CD) to Azo-MPEG both caused distinct changes, with all signals being altered from sharp to broad and shifted upfield, and protons H_b and H_c producing a large splitting (Figure S26b and d in the Supporting Information). These results were ascribed to the *trans*-Azo proton environment variation in the hydrophobic β-CD cavity. A similar result was reported by Yuan et al.[16]

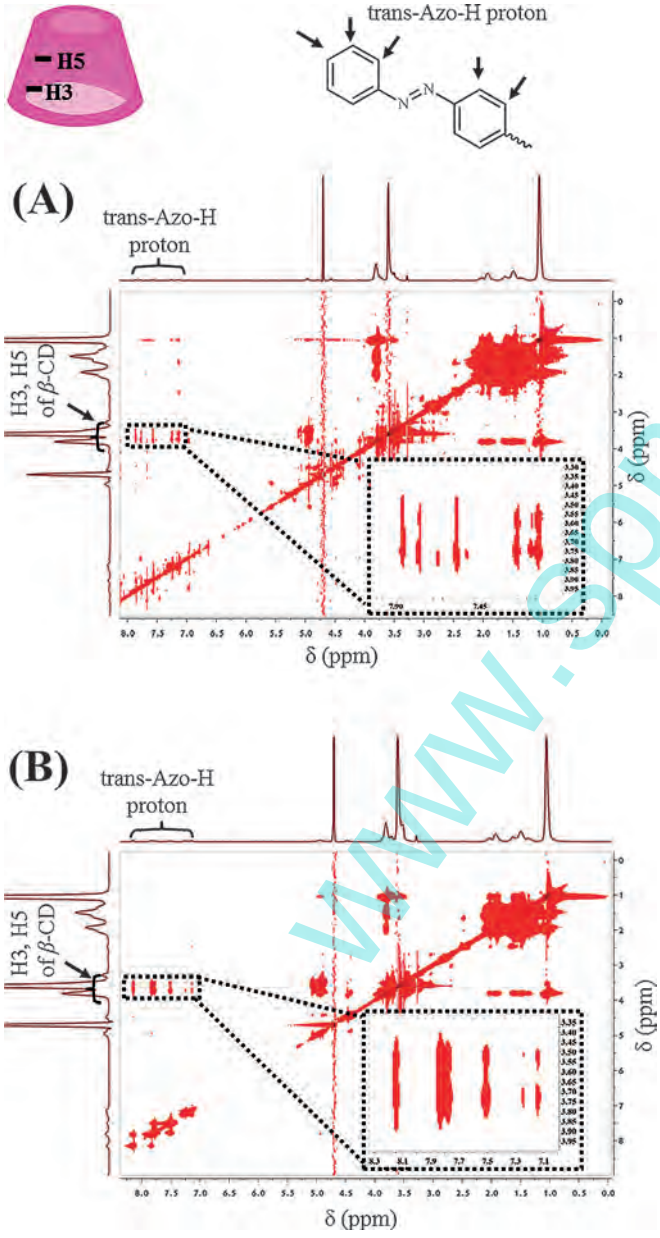

Figure 1. 2D NOESY NMR spectra of the supramolecular polymers SSP1 (A) and SSP2 (B) at 20 °C in D_2O (inset: partial enlargement).

To further confirm the formation and reversibility of host–guest complexes, UV/Vis absorption spectra of Azo-MPEG and Azo-2MPEG in the absence and presence of PNIPAM-2β-CD and PNIPAM-β-CD were measured. Generally, the absorption bands at $\lambda \approx 323$ and 432 nm can be ascribed to the π–π* transition (H aggregate) of the *trans* form and n–π* transition (J aggregate) of the *cis* form of the Azo group, respectively.[17] As shown in Figure 2 A, compared with the pure solution of Azo-2PEG, the absorption intensity at $\lambda \approx 323$ nm of mixed solutions of PNIPAM-β-CD and Azo-2MPEG was enhanced due to inclusion complexation between the *trans*-Azo group and β-CD units. Upon irradiation with UV light at $\lambda = 365$ nm for 15 min, the absorption band at $\lambda \approx 360$ nm decreased notably, whereas the absorption band at $\lambda \approx 450$ nm increased slightly; both were restored after exposure to visible light, which indicated that the photoisomerization of Azo caused a conformational change from the *trans* form to the *cis* form and was restored to the *trans* form.[17] Furthermore, the reversible photoisomerization of β-CD/Azo complexes could be repeatedly induced by alternating UV- and visible-light irradiation, as shown in Figure 2 C. A similar phenomenon was found for mixed solutions of PNIPAM-2(β-CD) and Azo-MPEG (Figure 2 B and D). Moreover, the dissociation of host–guest complexes induced by the photoisomerization of β-CD/Azo complexes was also confirmed by 2D NOESY NMR spectroscopy. As shown in Figure S27 in the Supporting Information, upon irradiation with UV light at $\lambda = 365$ nm for 15 min, no correlation between β-CD and Azo was observed, which indicated that the β-CD/Azo inclusion complexes dissociated in response to UV irradiation.

These results indicated that SSP1 and SSP2 with different numbers of host–guest binding sites formed. It should be noted that SSP1 and SSP2 were composed of approximate building blocks and block lengths with one temperature-sensitive PNIPAM arm ($DP_{PNIPAM\ in\ SSP1} = 46$, $DP_{PNIPAM\ in\ SSP2} = 44$) and two hydrophilic MPEG arms ($DP_{MPEG} = 22$). The corresponding SSP1 and SSP2 self-assemblies were obtained by heating the solutions above their LCSTs (Figure S28 in the Supporting Information). Thus, the influence of β-CD/Azo-based binding sites on the self-assembly behavior of SSP1 and SSP2 can be reasonably investigated in the presence of external stimuli, including temperature and irradiation. TEM, AFM, dynamic light scattering (DLS), fluorescence (FL) spectroscopy, and ^{1}H NMR spectroscopy (in D_2O) were performed to examine the binding-site-regulated self-assembly process.

TEM was used to visualize the morphology and size of the SSP1 and SSP2 self-assemblies by rapidly heating the solution of polymer from 20 °C to 37, 45, and 60 °C. As depicted in Figure 3 A–C and E–G, and Figure S29 in the Supporting Information, typical TEM images of these self-assemblies were obtained by drying aqueous solutions of samples on a copper grid without staining. Significant differences in morphologies and size were observed at different temperatures. No evident

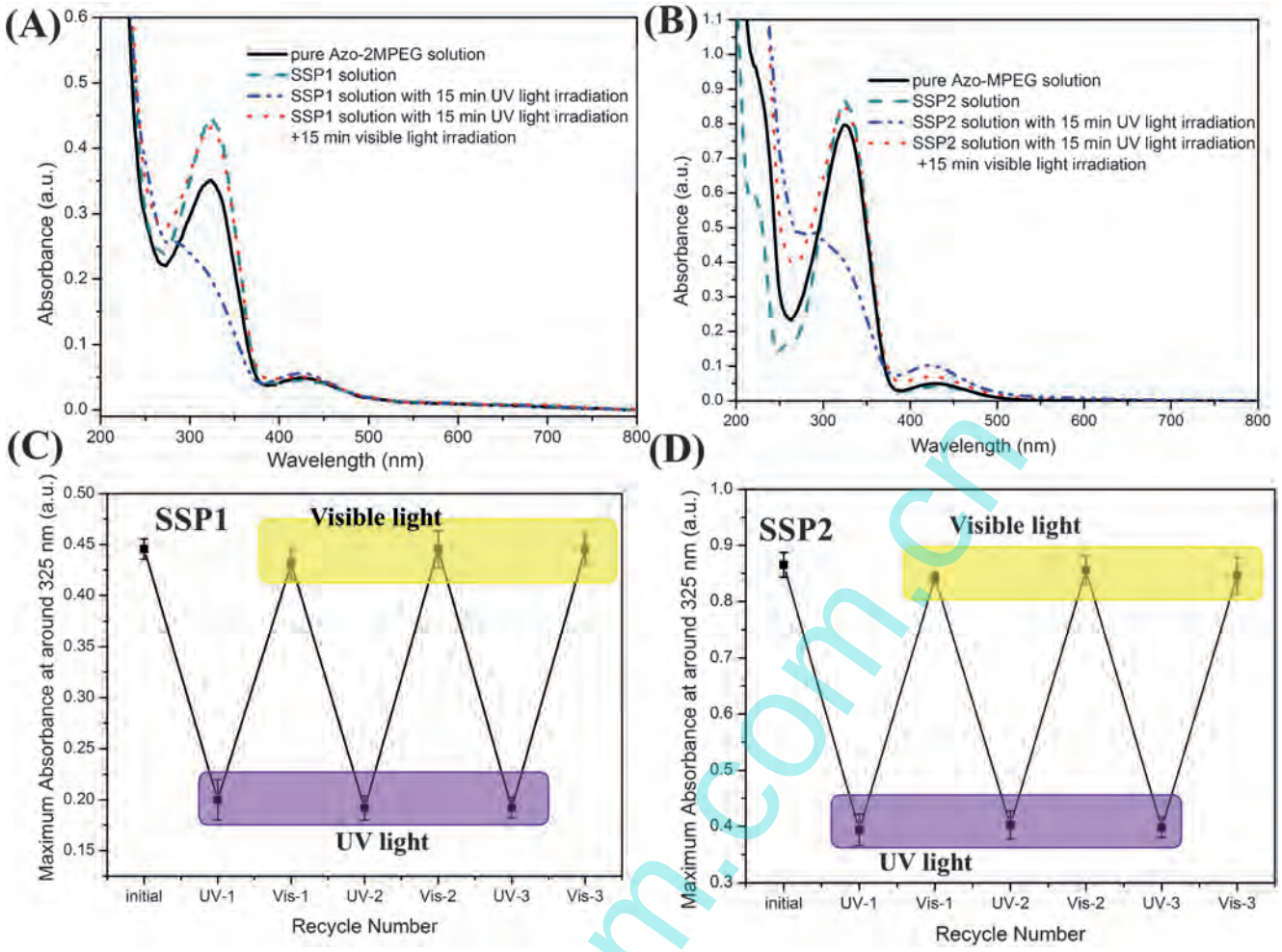

Figure 2. UV/Vis absorption spectra for the reversible photoisomerization of the Azo group in different aqueous solutions of polymer at 20 °C by irradiating with UV and visible light: A) solutions of pure Azo-2MPEG and SSP1; B) solutions of pure Azo-MPEG and SSP2. The changes to the UV absorbance at $\lambda = 360$ nm with alternate cycles of UV- and visible-light irradiation of solutions of SSP1 (C) and SSP2 (D). (Concentrations of SSP1 and SSP2 were constant at 2.5×10^{-5} M.)

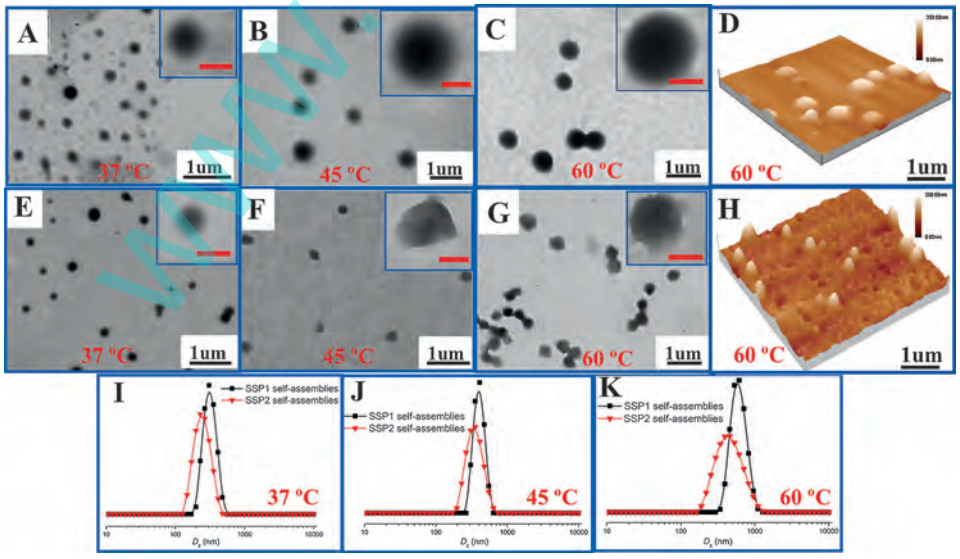

Figure 3. Typical TEM images of SSP1 (A–C) and SSP2 (E and G) self-assemblies obtained by rapid heating from 20 °C to 37, 45, or 60 °C at a polymer concentration of 1 mg mL^{-1} in H_2O (inset: enlarged images; scale bar: 200 nm). AFM images of SSP1 (D) and SSP2 (H) self-assemblies at 60 °C. DLS results (I–K) of samples in A)–C) and E)–G).

self-assemblies were found for SSP1 and SSP2 at room temperature (Figure S29 in the Supporting Information); however, SSP2 self-assemblies gradually presented a flower-like morphology (Figure 3E–G), whereas SSP1 self-assemblies retained a relatively regular spherical structure (Figure 3A–C) as the temperature increased. Notably, these morphological differences became more apparent at 60 °C (Figure 3G and C). Moreover, the average diameter ($D_{av,TEM}$) of SSP2 self-assemblies was smaller than those of SSP1 self-assemblies at 37, 45 and 60 °C (Table S2 in the Supporting Information). Similarly, the 3D AFM images indicated that SSP1 self-assemblies possessed more regularly spherical structures and bigger sizes than those of SSP2 self-assemblies (Figure 3D and H). For comparison, the hydrodynamic diameter (D_h) and diameter distributions of SSP1 and SSP2 self-assemblies at 37, 45, and 60 °C were determined by DLS (Figure 3I–K and Table S2 in the Supporting Information). The sizes of SSP1 and SSP2 self-assemblies are quite large. Similar results can be drawn from the related literature.[8g] One possible explanation is that the stabilization effect of the PEG corona on the PNIPAM cores is weaker than that of traditional CSPs, leading to easy aggregation during the dynamic exchange of the building blocks due to noncovalent bonds. The size of these self-assemblies displayed similar changes with increasing temperature as those observed by TEM. Furthermore, the D_h values of SSP2 self-assemblies were smaller than those of SSP1 self-assemblies. These results demonstrate that the β-CD/Azo binding site has a pronounced effect on the morphology and size of the SSP self-assemblies during heating.

The core–corona structures of SSP1 and SSP2 self-assemblies were further explored by ^{1}H NMR spectroscopy analysis in D_2O. As shown in Figure 4A–4B, when the solution temperature of SSP1 and SSP2 self-assemblies was gradually increased from 20 to 60 °C, signals corresponding to the PNIPAM segments (typical proton signals of r, k, q, and p corresponding to $\delta = 1.04$, 3.84, 1.97, and 1.44 ppm, respectively) attenuated dramatically and were shifted downfield, whereas the MPEG segments remained in the spectra. These results suggest that PNIPAM segments collapsed into the core after the temperature was elevated above the LCST of PNIPAM, whereas the MPEG segments formed the corona layer. The integral values of r (the methyl protons in the PNIPAM segments) to a (the methylene protons in the MPEG segments), representing the hydrophobic–hydrophilic proportions in the self-assemblies, were also calculated (Figure 4C). The r/a values of SSP1 and SSP2 self-assemblies first decreased and were then restored during the cooling process, which indicated that the hydrophobic–hydrophilic proportions first increased and then decreased. Furthermore, SSP1 self-assemblies showed much sharper attenuation and restoration than SSP2 self-assemblies, which indicated that they possessed different hydrophobic–hydrophilic contents, depending on the β-CD/Azo binding site during the heating–cooling process.

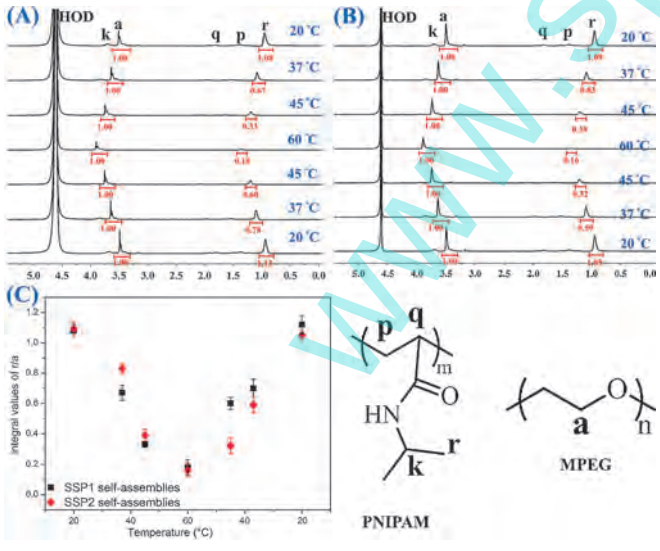

Figure 4. Variable-temperature ^{1}H NMR spectra of SSP1 and SSP2 self-assemblies upon rapid heating from 20 to 60 °C and then cooling back to 20 °C at a concentration of 1 mg mL^{-1} in H_2O: A) SSP1 self-assemblies; B) SSP2 self-assemblies. C) The fitted curves of the integral values of r (the methyl protons in PNIPAM segments) to a (the methylene protons in MPEG segments) corresponding to A) and B).

Subsequently, the temperature-induced dynamic self-assembly processes of SSP1 and SSP2 were investigated by in situ monitoring of the changes of D_h and I_1/I_3 values during heating, as determined by DLS and FL, respectively. At a slow heating rate of 1 K min^{-1}, the recorded D_h obtained by DLS analysis (Figure 5A) displayed the behavior expected from that reported in the literature.[9b,14c] Small particles with D_h below 10 nm were first observed below 30 °C. After heating above the LCSTs of SSP1 and SSP2, self-assemblies formed with D_h values of tens to hundreds of nanometers. Further heating led to agglomeration of the self-assemblies, accompanied by the generation of large aggregates with D_h values of over 1000 nm. Dehydration of the PNIPAM chains caused the size to increase constantly (first stage), then the stability of the PEG corona on the PNIPAM cores decreased, and finally the aggregates began to agglomerate or even precipitate (second stage).[9b,d] Although the overall D_h changes of these self-assemblies are similar due to similar PNIPAM block lengths of SSP1 and SSP2, the D_h growth processes were completely different. Compared with the stair-like D_h growth style of the SSP1 self-assemblies, the D_h of the SSP2 self-assemblies grew gradually with increasing temperature; this indicated that the self-assembly process of SSP2 was more stable than that of SSP1. FL spectroscopy was also performed to investigate the thermally induced self-assembly processes of SSP1 and SSP2 by using pyrene as a probe. Pyrene FL reports the polarity or hydrophobicity of the region at which it is solubilized.[18] The emission intensity ratio of the first to the third vibronic bands of the pyrene FL, usually defined as the I_1/I_3 ratio, has been widely used to study the formation and properties of aggregated systems. The I_1/I_3 value of the aqueous solution of pyrene in the presence of SSP1 and SSP2 during heating was recorded (Figure 5B). At 20 °C, the I_1/I_3 value of the aqueous solution of pyrene without the presence of the polymers was 1.413. After the addition of SSP1 and SSP2, the I_1/I_3 values of the two polymer solutions were slightly lower than that of the blank pyrene solution. This is attributed to the formation of hydrophobic domains by mild

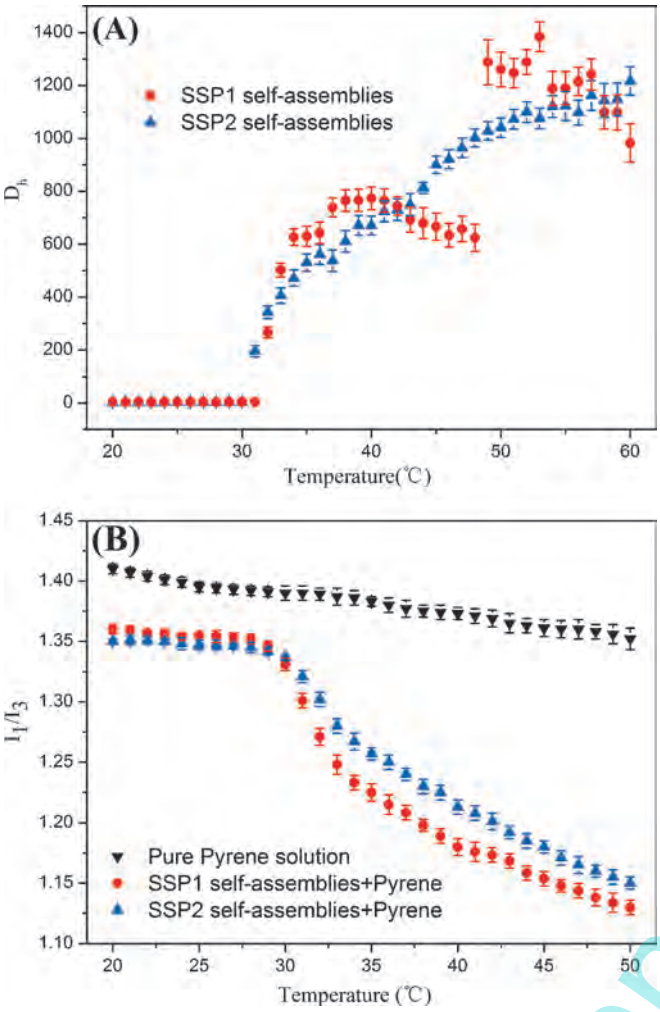

Figure 5. Investigation of the dynamic self-assembly processes of SSP1 and SSP2. A) Temperature-sequenced DLS measurements of SSP1 and SSP2 self-assemblies ([polymer]: 1 mg mL^{-1}; slow heating rate of 1 K min^{-1}). B) I_1/I_3 values of an aqueous solution of pyrene in the presence of SSP1 and SSP2 as a function of temperature ([polymer]: 1 mg mL^{-1}, [pyrene]: 6×10^{-7} mol L^{-1}).

aggregation of the backbone or nonhydrated side groups of PNIPAM. With increasing temperature, the I_1/I_3 values of the pyrene/polymers system both exhibit an abrupt decrease at the LCST, which indicates a significant decline in polarity and the sudden formation of hydrophobic domains in these self-assemblies. In comparison, the I_1/I_3 value of SSP1 decreased relatively sharply, whereas that of SSP2 displayed a smoother decrease, in accordance with the DLS results. The results indicate that the β-CD/Azo binding site could indeed influence the dynamic formation process of the SSP self-assemblies.

Additionally, the photo effects on the self-assembly processes of SSP1 and SSP2 during heating were investigated. Solutions of SSP1 and SSP2 were irradiated with UV light for 15 min at different temperatures, and the size and morphological changes to the self-assemblies were monitored by DLS and TEM (Figure 6 and Table S2 in the Supporting Information). Interestingly, an evident difference in the morphology and size of these self-assemblies was observed when solutions of polymer were exposed to UV light at 45 and 60 °C (Figure 6 B–C and E–F in comparison with Figure 3 B–C and F–G). SSP1 self-assemblies displayed clear coalescence, whereas SSP2 self-assemblies nearly retained their initial morphology, although their size decreased to some degree. The DLS data for SSP1 and SSP2 self-assemblies shown in Figure 6 G–I and Table S2 in the Supporting Information also gave similar results to those obtained by TEM. The results indicate that the effect of the β-CD/Azo binding site on the self-assembly process of SSP is more evident with UV-light irradiation than with increasing the temperature.

The influence of binding sites on the light-responsive drug-release functions of SSP1 and SSP2 self-assemblies was also investigated. As seen in Figure 7, these self-assemblies are good candidates for controlling the release of DOX molecules. DOX-loaded SSP1 and SSP2 self-assemblies both showed sustained release, and less than 20 % of DOX was released at 37 °C over 48 h. The cumulative release of DOX-loaded SSP2 self-assemblies at 48 h was 14.3 %, which was less than that of DOX-loaded SSP1 self-assemblies (19.5 %). Additionally, light has recently attracted much attention in drug-delivery systems, since it can be localized in time and space, and it can also be triggered from outside of the system.[15a,c] As shown in Figure 7 A, after UV-light irradiation, the cumulative release of DOX-loaded SSP1 self-assemblies incremented notably from 14.8 to 36.1 %, whereas DOX-loaded SSP2 self-assemblies only increased from 14.3 to 19.5 % over a period of 48 h. These results indicate that the release rate of DOX from SSP2 self-assemblies exhibits much better controllability than that of SSP1 self-assemblies, regardless of increasing temperature or UV-light irradiation.

The release mechanism of DOX from SSP1 and SSP2 self-assemblies was thus proposed to elucidate the release behavior by studying the release kinetics with a simple semiempirical equation [Eq. (1)] and a modified equation [Eq. (2)] to describe the release behavior of polymeric micelles.[19]

$$\frac{M_t}{M_\infty} = kt^n \quad (1)$$

$$\ln r = \ln k + n \ln t, \ldots r = M_t/M_\infty \quad (2)$$

in which M_t and M_∞ are the cumulative amounts of guest molecule released at time t and infinity, respectively; k is the release constant; k' is the constant proportional to k; and n describes the kinetic and release mechanism. For a diffusion–degradation controlled release system, for spherical particles n is usually between 0.43 and 0.85. When n is close to 0.43, diffusion, referred to as "Fickian diffusion", is the major driving force. When n is close to 0.85, the release is mainly controlled by degradation.[20] Based on the above deduction about the diffusion-controlled mechanism, Equation (2) can be obtained from Equation (1) by rearrangement and is more suitable for this release system. The results in Figure 7 B and Table 1 show that the cumulative release amount and release time of DOX-loaded SSP1 and SSP2 self-assemblies exhibit a linear correlation within the given range of time at 37 °C, with an R^2 value

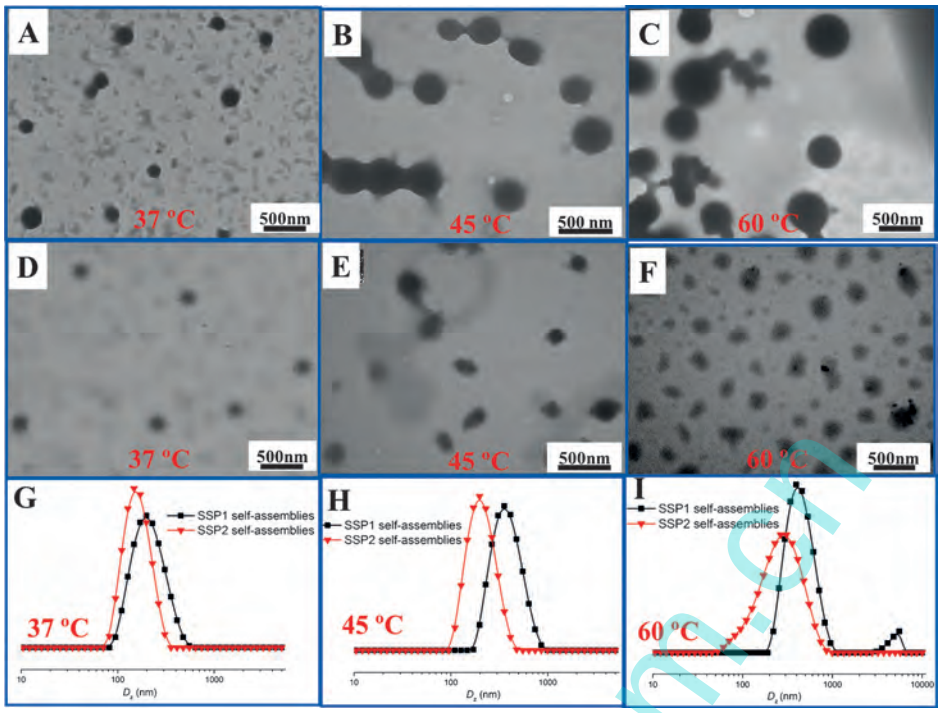

Figure 6. Typical TEM images of SSP1 (A–C) and SSP2 (D–F) self-assemblies upon UV irradiation for 15 min at 37, 45, and 60 °C with a polymer concentration of 1 mg mL^{-1} in H_2O. DLS results (G–I) for samples in A)–F).

Table 1. Release kinetics parameters of DOX from SSP1 and SSP2 self-assemblies with or without UV-light irradiation at 37 °C fitted with Peppas'[19] formula.[a]

Release sample	UV	Fitting equation	n[b]	k[b]	R^2[b]
DOX-loaded SSP1	without	$\ln r = 0.542 \ln t - 4.160$	0.542	0.016	0.966
DOX-loaded SSP2	without	$\ln r = 0.528 \ln t - 3.645$	0.528	0.026	0.990
DOX-loaded SSP1	with	$\ln r = 0.433 \ln t - 3.266$	0.433	0.038	0.985
DOX-loaded SSP2	with	$\ln r = 0.509 \ln t - 2.979$	0.509	0.051	0.986

[a] All experiments were conducted at 37 °C. [b] Calculated by using Equation (2).

equal or close to 0.99 and n close to 0.43. This result indicates that the release mechanism of DOX is mainly dominated by the diffusion-controlled mechanism. In particular, UV-light irradiation caused the n values to decrease for both DOX-loaded SSP1 and SSP2 self-assemblies, from 0.542 to 0.433 for SSP1 self-assemblies and a slighter decrease from 0.528 to 0.509 for SSP2 self-assemblies. These decreases indicated that the dominance of the diffusion mechanism increased to a greater extent for the DOX-loaded SSP1 self-assemblies than that for the SSP2 self-assemblies after UV-light irradiation due to the effect of β-CD/Azo binding sites.

These results collectively indicate that the β-CD/Azo binding site can affect the self-assembly process and function of SSPs with dual thermo- and photoresponsiveness in aqueous solutions, and a corresponding mechanism was proposed (Scheme 1). The main reason for the differences between the self-assembly morphology and size, as well as controlled release rates of DOX, of SSP1 and SSP2 may be attributed to the cooperativity generated by the adjacent β-CD/Azo binding sites. Generally, cooperativity takes place when multiple intermolecular binding interactions of a monovalent ligand to a polyvalent macromolecule occur.[12a] Positive cooperativity is evidenced by a statistically normalized enhancement of binding strength.[12b,c] Herein, positive cooperativity generated by the adjacent β-CD/Azo binding sites leads to the stronger binding strength of SSP2 than that of SSP1 (Scheme 1 A and A′). When the solution was heated above the LCST of the PNIPAM segment, the β-CD/Azo binding sites were distributed onto different surfaces of the SSP1 and SSP2 self-assemblies. The surfaces of SSP2 self-assemblies have a higher β-CD/Azo binding-site distribution density than that of SSP1 self-assemblies (Scheme 1 A–B and A′–B′). Thus, the cooperativity of SSP2 self-assemblies is enhanced. During further heating, enhanced cooperativity on the hydrophilic shell layer of SSP2 self-assemblies plays an important role in steadying the hydrophobic core layer, compared with that in the SSP1 self-assemblies (Scheme 1 B–C and B′–1C′). As a result, the smaller, flower-like morphology of the SSP2 self-assemblies formed at 60 °C compared with SSP1 self-assemblies with regularly spherical structures and bigger sizes (Scheme 1 C–D and C′–D′). Furthermore, when these self-assemblies were irradiated by UV light at 60 °C, enhanced cooperativity endows the SSP2 self-assemblies with a more stable self-assembly state and avoids coalescence compared with the SSP1 self-assemblies (Scheme 1 D–E and 1D′–E′). Based on this analysis, enhanced cooperativity can fur-

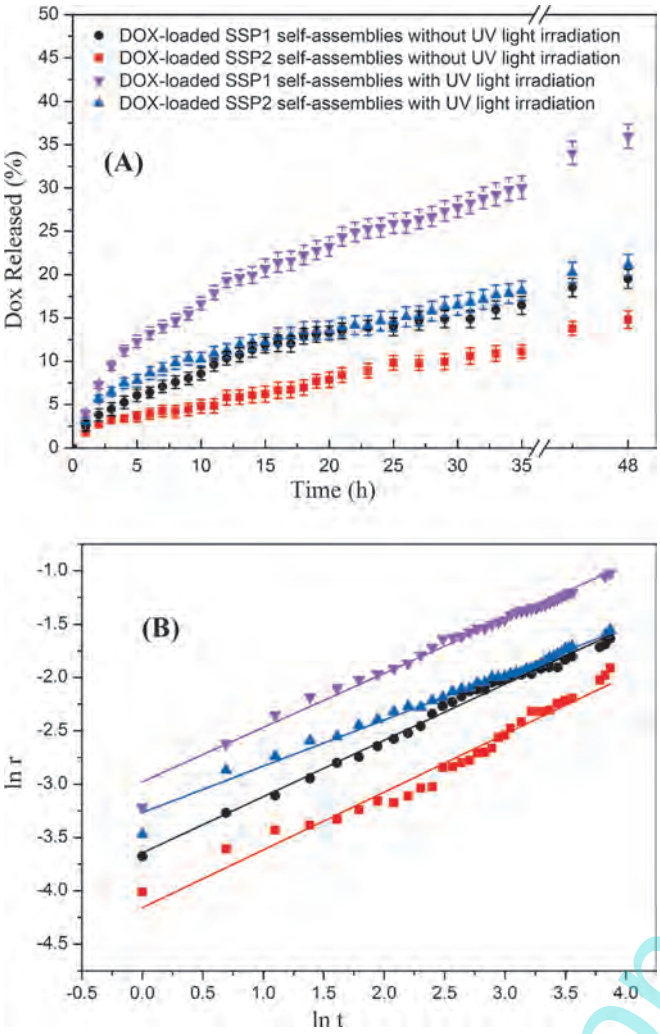

Figure 7. Cumulative release curves of DOX from SSP1 and SSP2 self-assemblies as a function of time over a period of 48 h: A) with or without UV light irradiation for 15 min at 37 °C; B) corresponding fitted curves for release kinetics.

ther induce better controllability of the DOX-release behavior from SSP2 self-assemblies than that of SSP1 self-assemblies, regardless of increasing temperature or UV-light irradiation. In summary, cooperativity exists between two adjacent β-CD/Azo binding sites and dominates tuning of the self-assembly and function of the SSP.

To further confirm the existence of this cooperativity, we utilized isothermal titration calorimetry (ITC) and UV/Vis spectroscopy measurements to determine the initial association constants (K_t) of β-CD/Azo host–guest binding sites in SSP1 and SSP2. In a typical ITC experiment, an aqueous solution of β-CD-PNIPAM (12.0 mM) was trickled into a solution of Azo-2MPEG (0.6 mM), and an exothermic binding isotherm was obtained (Figure 8A). The data yielded the binding constant, K_t, for SSP1 of $0.92\times10^3\ M^{-1}$. Similarly, the K_t value of SSP2 was calculated to be $3.95\times10^3\ M^{-1}$ at the same concentration of β-CD and Azo. The results indicate that the K_t of β-CD/Azo in SSP2 is significantly higher than that of SSP1, which confirms the existence of positive cooperativity in the two adjacent binding sites of SSP2.

UV/Vis measurements were also performed to determine K_t. When the *trans*-Azo concentration of Azo-2(MPEG) (Figure 9A) and Azo-MPEG (Figure 9C) was maintained at 1×10^{-5} M, the absorption of *trans*-Azo at $\lambda = 322$ nm markedly increased with increasing PNIPAM-β-CD and PNIPAM-2(β-CD) concentrations. With an assumption of 1:1 stoichiometry, inclusion complexation of PNIPAM-β-CD (H) with Azo-2(MPEG) (G) and PNIPAM-2(β-CD) (H) with Azo-MPEG (G) is expressed by Equation (3):

$$H + G \xrightarrow{K_t} H \cdot G \tag{3}$$

The double reciprocal plot was utilized through the modified Hildebrand–Benesi equation [Eq. (4)]:

$$\frac{1}{(\Delta A)} = \frac{1}{K_t \Delta_\varepsilon [H][G]} + \frac{1}{\Delta\varepsilon[H]} \tag{4}$$

in which H, G, and K_t represent the host, guest, and association constants, respectively; ΔA denotes the absorbance difference before and after the addition of the β-CD species; and $\Delta\varepsilon$ denotes the difference of the molar extinction coefficient between the host and host–guest complex at the same wavelength. The association constant, K_t, of SSP2 calculated by the equation is $8.25\times10^3\ M^{-1}$, which is higher than that of the SSP1 complex ($2.96\times10^3\ M^{-1}$) and in accordance with the ITC results. Such a difference in K_t values implies that the binding strength of SSP2 with positive cooperativity is stronger than that of SSP1 without cooperativity.

The zeta potential was used to further confirm the enhanced cooperativity of SSP2 self-assemblies during heating through determining the distribution density of β-CD/Azo binding sites on the surfaces of the self-assemblies. According to published work[2a] and our own prior reports,[21] adamantane (Ada) can form inclusion complexes with β-CD and its β-CD inclusion constant is higher than that of Azo/β-CD. Thus, Ada–COONa was used as a guest molecule to monitor the surface charge of the self-assemblies. As shown in Figure 10, the zeta-potential values of SSP1 and SSP2 self-assemblies decreased upon the addition of Ada–COONa (0.2 mM) while increasing the temperature. By comparison, SSP2 self-assemblies with Ada–COONa had a higher surface charge than those of SSP1 self-assemblies at the temperatures tested. The higher charge values of SSP2 self-assembly surfaces can be attributed to the greater number of β-CD/Ada–COO^- inclusion complex sites during heating. This result directly confirmed that the surfaces of SSP2 self-assemblies possessed a higher distribution density of β-CD/Azo binding sites than those of SSP1 self-assemblies. Thus, the cooperativity of SSP2 self-assembly surfaces was clearly enhanced.

Conclusion

Two dual-stimuli thermo- and photoresponsive supramolecular Y-shaped polymers containing one or two binding sites (SSP1 or SSP2, respectively) were successfully synthesized by combin-

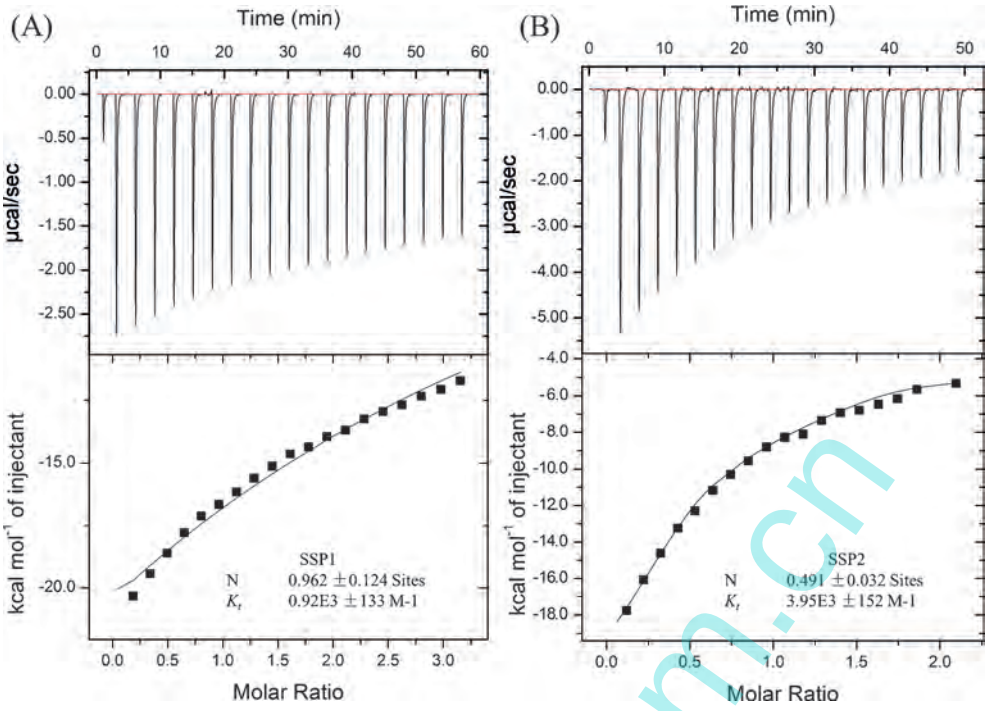

Figure 8. Typical ITC curves corresponding to the binding interaction of SSP1 (A) and SSP2 (B) in aqueous solution at 20 °C. Top panels show exothermic heat flows that are released upon successive injection of aliquots (10 µL) of PNIPAM-β-CD into AZO-2MPEG or PNIPAM-2(β-CD) into AZO-MPEG. Bottom panels show integrated heat data, which give a differential binding curve that was fitted to a standard single-site binding model.

ing RAFT polymerization and click chemistry. Compared with the SSP1 self-assemblies, SSP2 self-assemblies exhibited a flower-like morphology and smaller size with increasing polymer solution temperature. SSP2 self-assemblies also exhibited a much more stable self-assembly process than that of SSP1 self-assemblies when the polymer solutions were heated or irradiated with UV light. The release behavior of DOX from SSP2 self-assemblies is much more controllable than that of SSP1 self-assemblies, regardless of increasing temperature or UV light irradiation. The positive cooperativity generated by the two adjacent β-CD/Azo binding sites of SSP2 contributed to tuning of the self-assembly behavior and drug-release function. The positive cooperativity could be further enhanced when self-assemblies with a high binding-site distribution density formed. Our study is expected to be further used to generalize the design of novel supramolecular polymer systems with precisely controlled self-assembly parameters and adjust functional applications in smart drug delivery and biomedicine.

Experimental Section

Materials

4-Phenylazobenzoyl chloride (TCI, 98%), *N*-isopropylacrylamide (NIPAM; Acros, 99%), and pyrene (Alfa Aesar, 99%) were used as received. 4-Dimethylaminopyridine (DMAP; 99%), doxorubicin hydrochloride (DOX·HCl; 98%), *N,N*-dicyclohexylcarbodiimide (DCC; 95%), *N*-hydroxysuccinimide (NHS, 95%), and triethylamine (TEA) were from Sinopharm Chemical Reagent Co., Ltd., Shanghai, P.R. China. Pyrene (98%) was purchased from Adamas-beta. *N,N,N′,N″,N‴*-Pentamethyldiethylenetriamine (PMDETA, 98%) was supplied by Yutian Chemical Co., Ltd., Liyang, P.R. China. 2,2′-Azobis(isobutyronitrile) (AIBN; Fluka, 99%) was recrystallized twice from methanol. CuBr (Aladdin, 99%) was purified by being stirred in acetic acid overnight. After filtration, it was washed with ethanol and diethyl ether and then dried in a vacuum oven at room temperature. MPEG (M_n = 1000 Da, Aladdin) was dried by azeotropic distillation in the presence of toluene. 1,4-Dioxane, $CHCl_3$, CH_2Cl_2, and DMF, were dried with a 3 Å grade molecular sieves before use.

Formation of SSP1 and SSP2 through β-CD/Azo interactions

Azo-MPEG (6.0 mg, 1.0 equiv) was dissolved in DMF (2.0 mL) and added dropwise to a solution of PNIPAM-2β-CD (18.0 mg, 1.0 equiv) in DMF (2.0 mL) under vigorous stirring. Similarly, Azo-2MPEG (6.0 mg, 1.0 equiv) was dissolved in DMF (2.0 mL) and added dropwise to a solution of PNIPAM-β-CD (12.0 mg, 1.0 equiv) in DMF (2.0 mL) under vigorous stirring. The resulting solution was dialyzed against a mixture of deionized water/DMF. The water content was gradually changed from 70 to 100% over 1 day and dialysis was continued for 3 days with deionized water at 4 °C. The solvent was removed in vacuo to yield the supramolecular copolymer in quantitative yield.

Polymer structure characterization

FTIR spectra were recorded on a Nicolet iS10 IR spectrometer (Nicolet USA) by casting samples into thin films on KBr. Transition mode was used and the wavenumber range was set from $\tilde{\nu}$ = 4000 to 500 cm^{-1}. ^1H and ^{13}C NMR spectra were recorded on a Bruker Avance 300 spectrometer (Bruker BioSpin, Switzerland) operating at 400 MHz (^1H) in $CDCl_3$, [D_6]DMSO, or D_2O. 2D NOSEY was performed on a Bruker Avance III 400 spectrometer operating at 400 MHz. ESI-MS was recorded by using a microTOF-QII 10280 spectrometer (Varian Inc., USA). The molecular structure parame-

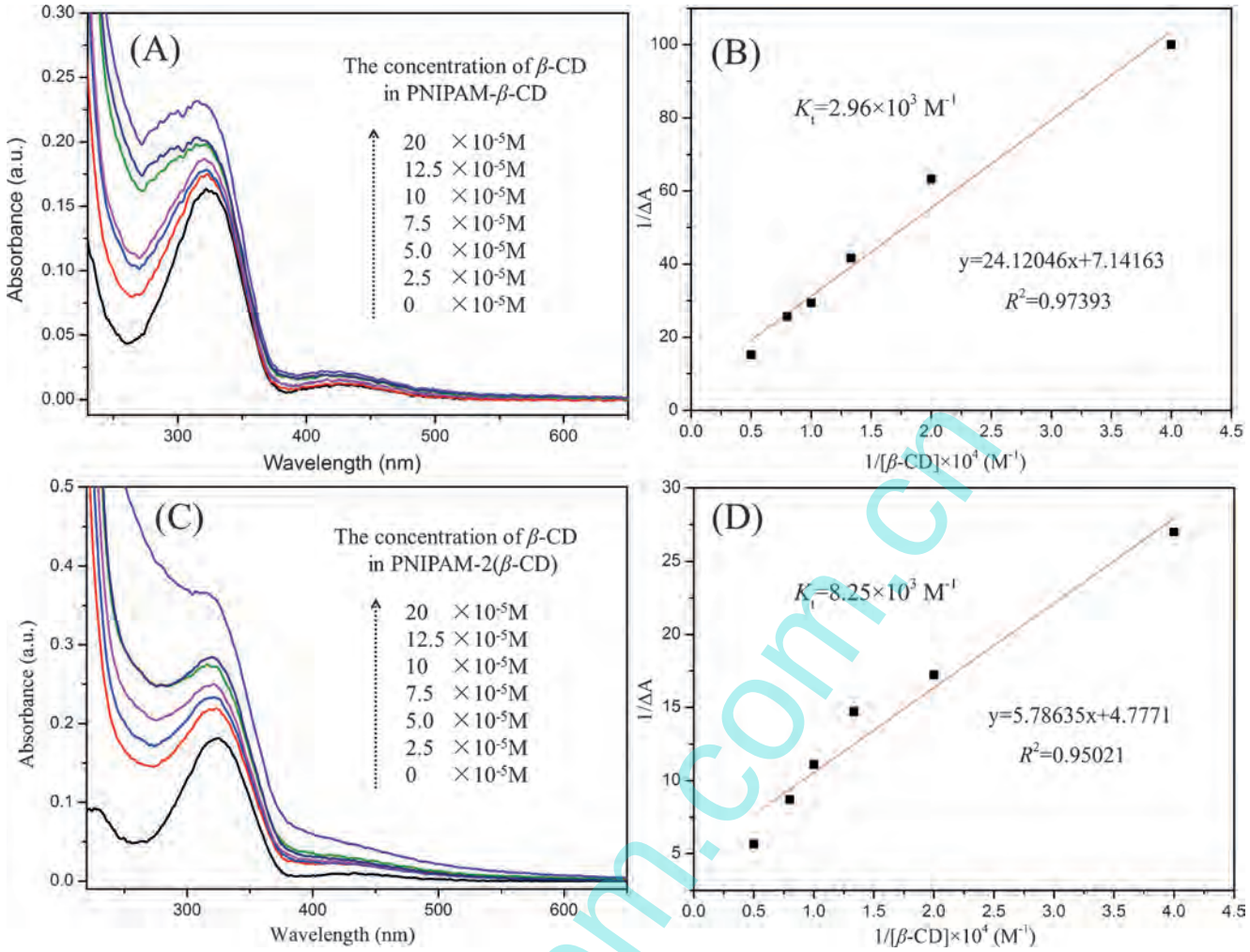

Figure 9. UV absorption spectra of *trans*-Azo upon the stepwise addition of β-CD species to determine the binding interactions of SSP1 (A, B) and SSP2 (C, D). The concentration of Azo-MPEG and Azo-(2MPEG) was kept at 1×10^{-5} M for the stepwise addition of PNIPAM-β-CD (A) and PNIPAM-2(β-CD) (C); double reciprocal plots of Azo-2(MPEG)/PNIPAM-β-CD (B) and Azo-MPEG/PNIPAM-2(β-CD) (D) are also shown.

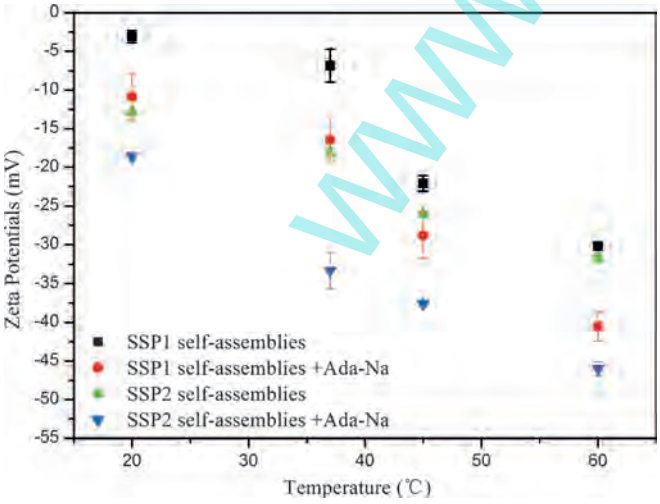

Figure 10. Change in the zeta-potential values on the surfaces of SSP1 and SSP2 self-assemblies in aqueous solution before and after the addition of Ada–COONa at various temperatures ([polymer] = 1 mg mL^{-1}).

ters of the resulting polymers were determined on a DAWN EOS SEC/MALLS instrument. HPLC-grade DMF containing LiCl (0.01 mol L^{-1}; at 40 °C) or THF (at 25 °C) was used as the eluent at a flow rate of 0.5 mL min^{-1}. The chromatographic system consisted of a Waters 515 pump, differential refractometer (Optilab rEX), and one-column MZ 10^3 Å 300×8.0 mm for the DMF system or two-column MZ 10^3 Å and 10^4 Å for the THF system. The MALLS detector (DAWN EOS), quasi-elastic light scattering (QELS), and differential viscosity meter (ViscoStar) were placed between the SEC and the refractive index detector. The molecular weight (M_w) and molecular weight distribution (MWD) were determined by using a SEC/DAWN EOS/OptilabrEX/QELS instrument. ASTRA software (Version 5.1.3.0) was utilized for acquisition and analysis of data.

SSP self-assembly characterization

TEM observations were conducted on a Hitachi H-7650 electron microscope at an acceleration voltage of 70 kV. Samples were prepared by dropping micellar solution (10 μL) onto copper grids without staining, followed by quenching with liquid nitrogen and freeze-drying in vacuum. The heating speed was kept at 20 °C min^{-1} and then the micellar solution was stable at a predetermined temperature for 5 min. The morphology was visualized by

means of AFM in tapping mode with a Nanowizard II controller (Benyuan, CSPM 5500, P.R. China). Tip information: radius ≤ 33 mm, cantilever length 10 mm, width 100 mm, thickness 30 mm, resonant frequency 300 kHz, and force constant 40 N m^{-1}. The size and size distribution of the aggregates at various temperatures were determined by DLS by using a Malvern Zetasizer Nano ZS instrument. The polymer solutions (1 mg mL^{-1}) were passed through a 0.45 μm microfilter and kept at a predetermined temperature for 5 min before measurements. The scattered light of a vertically polarized He–Ne laser ($\lambda = 633$ nm) was measured at an angle of 173° and collected on an autocorrelator. The pyrene inclusion behavior of polymers was determined by FL spectroscopy (Hitachi F-4600). The emission spectra of micellar solutions with a polymer concentration range from 1 to 1×10^{-4} mg mL^{-1} and a fixed pyrene concentration of 6×10^{-6} M were recorded from $\lambda = 355$ to 550 nm with an excitation wavelength of $\lambda = 335$ nm. The emission intensity ratio of the first vibronic band to that of the third of the spectra (I_1/I_3 ratio) was calculated and plotted against the polymer concentration. The LCSTs of the polymers were determined by UV/Vis spectroscopy (Shimadzu UV-2550 model, Japan) at $\lambda = 600$ nm. The transmittance of the aqueous solutions of polymer (1 mg mL^{-1}) was recorded at temperatures from 25 to 50 °C. Sample cells were thermostated with an external constant temperature controller. The temperature ramp was set at 0.33 °C min^{-1}. The temperature corresponding to the onset of the decrease in transmittance was defined as the LCST.

Drug-releasing behavior of SSP self-assemblies

To prepare DOX-loaded micelles, DOX·HCl was first stirred with excess TEA (2 equiv DOX·HCl) in dichloromethane overnight, extracted with $CHCl_3$, and dried in vacuo to give the free DOX base. Then, SSP1 or SSP2 self-assemblies (20 mg) were dissolved in DMF/H_2O (1.5 mL, 1:2), followed by sonication for 5 min to ensure sufficient inclusion complexation. Upon stirring, DMF (0.5 mL) containing DOX (2.01 mg) was added dropwise to the solution of inclusion complex in 3 min at 20 °C. The resulting solution was stirred for another 3 h at 37 °C to form the micellar solution. Deionized water (18.0 mL) was then added by syringe at a low rate over a period of 1 h. DOX that was not loaded into the self-assemblies was then removed by dialysis (MWCO 5000 dialysis bags) against deionized water for 48 h at 37 °C, and fresh deionized water was replaced approximately every 6 h. The drug release of the self-assemblies in phosphate-buffered saline (PBS; pH 7.4) was determined as follows: drug-loaded self-assembly solution (2 mL, 10 mg mL^{-1}) was injected into a dialysis bag (MWCO 5000) at 37 °C, and dialyzed against PBS under two different conditions (37 °C in PBS for 48 h; and 37 °C in PBS with UV irradiation for 48 h). At certain time intervals, PBS medium (4 mL) was removed and replaced by fresh PBS (4 mL). The amount of DOX in the solution was determined by UV/Vis spectrometry at $\lambda = 485$ nm.

Acknowledgements

This work was supported by the National Science Foundation of China (no. 21374088). W.T. acknowledges grants from the Program for New Century Excellent Talents of Ministry of Education (NCET-13-0476), the Key Laboratory Program of Science and Technology Coordinator Innovation Project of Shaanxi Province of China (2013SZS17-P01), and the Fundamental Research Funds for the Central Universities (3102015ZY096).

Keywords: cyclodextrins · host–guest systems · polymers · self-assembly · supramolecular chemistry

[1] a) T. Aida, E. W. Meijer, S. I. Stupp, *Science* **2012**, *335*, 813–817; b) E. A. Appel, J. Del Barrio, X. J. Loh, O. A. Scherman, *Chem. Soc. Rev.* **2012**, *41*, 6195–6214; c) A. Harada, Y. Takashima, M. Nakahata, *Acc. Chem. Res.* **2014**, *47*, 2128–2140; d) B. Rybtchinski, *ACS Nano* **2011**, *5*, 6791–6818; e) X. Ma, H. Tian, *Acc. Chem. Res.* **2014**, *47*, 1971–1981; f) L. Yang, X. Tan, Z. Wang, X. Zhang, *Chem. Rev.* **2015**, *115*, 7196–7239; g) X. Yan, F. Wang, B. Zheng, F. Huang, *Chem. Soc. Rev.* **2012**, *41*, 6042–6065; h) J. Hu, S. Liu, *Acc. Chem. Res.* **2014**, *47*, 2084–2095; i) R. Dong, Y. Zhou, X. Zhu, *Acc. Chem. Res.* **2014**, *47*, 2006–2016; j) X. Ji, S. Dong, P. Wei, D. Xia, F. Huang, *Adv. Mater.* **2013**, *25*, 5725–5729; k) S. Dong, Y. Luo, X. Yan, B. Zheng, X. Ding, Y. Yu, Z. Ma, Q. Zhao, F. Huang, *Angew. Chem. Int. Ed.* **2011**, *50*, 1905–1909; *Angew. Chem.* **2011**, *123*, 1945–1949; l) X. Ji, Y. Yao, J. Li, X. Yan, F. Huang, *J. Am. Chem. Soc.* **2013**, *135*, 74–77.

[2] a) E. Kolomiets, E. Buhler, S. J. Candau, J. M. Lehn, *Macromolecules* **2006**, *39*, 1173–1181; b) O. A. Scherman, G. B. W. L. Ligthart, R. P. Sijbesma, E. W. Meijer, *Angew. Chem. Int. Ed.* **2006**, *45*, 2072–2076; *Angew. Chem.* **2006**, *118*, 2126–2130; c) S. Liu, H. Zhu, H. Zhao, M. Jiang, C. Wu, *Langmuir* **2000**, *16*, 3712–3717; d) L. C. Gilday, S. W. Robinson, T. A. Barendt, M. J. Langton, B. R. Mullaney, P. D. Beer, *Chem. Rev.* **2015**, *115*, 7118–7195.

[3] a) U. S. Schubert, C. Eschbaumer, *Angew. Chem. Int. Ed.* **2002**, *41*, 2892–2926; *Angew. Chem.* **2002**, *114*, 3016–3050; b) P. R. Andres, U. S. Schubert, *Adv. Mater.* **2004**, *16*, 1043–1068; c) A. O. Moughton, R. K. O'Reilly, *J. Am. Chem. Soc.* **2008**, *130*, 8714–8725; d) G. R. Whittell, M. D. Hager, U. S. Schubert, I. Manners, *Nat. Mater.* **2011**, *10*, 176–188.

[4] a) A. Harada, R. Kobayashi, Y. Takashima, A. Hashidzume, H. Yamaguchi, *Nat. Chem.* **2011**, *3*, 34–37; b) U. Rauwald, O. A. Scherman, *Angew. Chem. Int. Ed.* **2008**, *47*, 3950–3953; *Angew. Chem.* **2008**, *120*, 4014–4017; c) X. Liao, G. Chen, X. Liu, W. Chen, F. Chen, M. Jiang, *Angew. Chem. Int. Ed.* **2010**, *49*, 4409–4413; *Angew. Chem.* **2010**, *122*, 4511–4515; d) Y. Liu, Y. Yu, J. Cao, Z. Wang, X. Zhang, *Angew. Chem. Int. Ed.* **2010**, *49*, 6576–6579; *Angew. Chem.* **2010**, *122*, 6726–6729; e) X. Yan, D. Xu, X. Chi, J. Chen, S. Dong, X. Ding, Y. Yu, F. Huang, *Adv. Mater.* **2012**, *24*, 362–369; f) G. Yu, K. Jie, F. Huang, *Chem. Rev.* **2015**, *115*, 7240–7303; g) Y. Chen, Y. Liu, *Chem. Soc. Rev.* **2010**, *39*, 495–505; h) C. Tu, L. Zhu, P. Li, Y. Chen, Y. Su, D. Yan, X. Zhu, G. Zhou, *Chem. Commun.* **2011**, *47*, 6063–6065; i) M. Zhang, D. Xu, X. Yan, J. Chen, S. Dong, B. Zheng, F. Huang, *Angew. Chem. Int. Ed.* **2012**, *51*, 7011–7015; *Angew. Chem.* **2012**, *124*, 7117–7121.

[5] a) L. E. Buerkle, S. J. Rowan, *Chem. Soc. Rev.* **2012**, *41*, 6089–6102; b) A. Feng, J. Yuan, *Macromol. Rapid Commun.* **2014**, *35*, 767–779.

[6] a) Y. Wang, H. Xu, X. Zhang, *Adv. Mater.* **2009**, *21*, 2849–2864; b) D. Koda, T. Maruyama, N. Minakuchi, K. Nakashima, M. Goto, *Chem. Commun.* **2010**, *46*, 979–981; c) H. Wang, S. Wang, H. Su, K. Chen, A. L. Armijo, W. Lin, Y. Wang, J. Sun, K. Kamei, J. Czernin, C. G. Radu, H. Tseng, *Angew. Chem. Int. Ed.* **2009**, *48*, 4344–4348; *Angew. Chem.* **2009**, *121*, 4408–4412; d) Z. Zhang, K. L. Liu, J. Li, *Macromolecules* **2011**, *44*, 1182–1193.

[7] a) W. Weng, Z. Li, A. M. Jamieson, S. J. Rowan, *Macromolecules* **2009**, *42*, 236–246; b) C. Po, A. Y. Tam, K. M. Wong, V. W. Yam, *J. Am. Chem. Soc.* **2011**, *133*, 12136–12143; c) S. P. Nunes, M. Karunakaran, N. Pradeep, A. R. Behzad, B. Hooghan, R. Sougrat, H. He, K. Peinemann, *Langmuir* **2011**, *27*, 10184–10190; d) Q. Lu, C. G. Bazuin, *Nano Lett.* **2005**, *5*, 1309–1314; e) Q. Jin, L. Zhang, M. Liu, *Chem. Eur. J.* **2013**, *19*, 9234–9241.

[8] a) D. Kurouski, X. Lu, L. Popova, W. Wan, M. Shanmugasundaram, G. Stubbs, R. K. Dukor, I. K. Lednev, L. A. Nafie, *J. Am. Chem. Soc.* **2014**, *136*, 2302–2312; b) M. Nakahata, Y. Takashima, A. Hashidzume, A. Harada, *Angew. Chem. Int. Ed.* **2013**, *52*, 5731–5735; *Angew. Chem.* **2013**, *125*, 5843–5847; c) Y. Wang, P. Han, H. Xu, Z. Wang, X. Zhang, A. V. Kabanov, *Langmuir* **2010**, *26*, 709–715; d) D. Wang, Y. Su, C. Jin, B. Zhu, Y. Pang, L. Zhu, J. Liu, C. Tu, D. Yan, X. Zhu, *Biomacromolecules* **2011**, *12*, 1370–1379; e) Z. Ge, S. Liu, *Macromol. Rapid Commun.* **2013**, *34*, 922–930; f) B. Liang, R. Tong, Z. Wang, S. Guo, H. Xia, *Langmuir* **2014**, *30*, 9524–9532; g) Y. Kang, Y. Ma, S. Zhang, L. Ding, B. Li, *ACS Macro Lett.* **2015**, *4*, 543–547.

[9] a) B. V. K. J. Schmidt, M. Hetzer, H. Ritter, C. Barner-Kowollik, *Prog. Polym. Sci.* **2014**, *39*, 235 – 249; b) B. V. K. J. Schmidt, M. Hetzer, H. Ritter, C. Barner-Kowollik, *Macromolecules* **2013**, *46*, 1054 – 1065; c) B. V. K. J. Schmidt, M. Hetzer, H. Ritter, C. Barner-Kowollik, *Polym. Chem.* **2012**, *3*, 3064 – 3067; d) B. V. K. J. Schmidt, C. Barner-Kowollik, *Polym. Chem.* **2014**, *5*, 2461 – 2472.
[10] Y. Liu, C. Yu, H. Jin, B. Jiang, X. Zhu, Y. Zhou, Z. Lu, D. Yan, *J. Am. Chem. Soc.* **2013**, *135*, 4765 – 4770.
[11] Q. Yan, J. Yuan, Z. Cai, Y. Xin, Y. Kang, Y. Yin, *J. Am. Chem. Soc.* **2010**, *132*, 9268 – 9270.
[12] a) J. D. Badjić, A. Nelson, S. J. Cantrill, W. B. Turnbull, J. F. Stoddart, *Acc. Chem. Res.* **2005**, *38*, 723 – 732; b) G. Ercolani, *J. Am. Chem. Soc.* **2003**, *125*, 16097 – 16103; c) A. Perl, A. Gomez-Casado, D. Thompson, H. H. Dam, P. Jonkheijm, D. N. Reinhoudt, J. Huskens, *Nat. Chem.* **2011**, *3*, 317 – 322.
[13] a) H. Zhang, X. Fan, R. Suo, H. Li, Z. Yang, W. Zhang, Y. Bai, H. Yao, W. Tian, *Chem. Commun.* **2015**, *51*, 15366 – 15369; b) Z. Yang, X. Fan, W. Tian, D. Wang, H. Zhang, Y. Bai, *Langmuir* **2014**, *30*, 7319 – 7326; c) H. Li, X. Fan, W. Tian, H. Zhang, W. Zhang, Z. Yang, *Chem. Commun.* **2014**, *50*, 14666 – 14669.
[14] a) H. G. Schild, *Prog. Polym. Sci.* **1992**, *17*, 163 – 249; b) H. Cheng, L. Shen, C. Wu, *Macromolecules* **2006**, *39*, 2325 – 2329; c) F. Sakai, G. Chen, M. Jiang, *Polym. Chem.* **2012**, *3*, 954 – 961.
[15] a) J. Gohy, Y. Zhao, *Chem. Soc. Rev.* **2013**, *42*, 7117 – 7129; b) D. Qu, Q. Wang, Q. Zhang, X. Ma, H. Tian, *Chem. Rev.* **2015**, *115*, 7543 – 7588; c) E. Fleige, M. A. Quadir, R. Haag, *Adv. Drug Delivery Rev.* **2012**, *64*, 866 – 884.
[16] Q. Yan, Y. Xin, R. Zhou, Y. Yin, J. Yuan, *Chem. Commun.* **2011**, *47*, 9594 – 9596.
[17] R. Dong, Y. Liu, Y. Zhou, D. Yan, X. Zhu, *Polym. Chem.* **2011**, *2*, 2771 – 2774.
[18] a) K. Kalyanasundaram, J. K. Thomas, *J. Am. Chem. Soc.* **1977**, *99*, 2039 – 2044; b) M. Murugesan, M. A. Scibioh, R. Jayakumar, *Langmuir* **1999**, *15*, 5467 – 5473.
[19] J. Siepmann, N. A. Peppas, *Adv. Drug Delivery Rev.* **2001**, *48*, 139 – 157.
[20] X. Q. Yang, J. J. Grailer, S. Pilla, D. A. Steeber, S. Q. Gong, *Bioconjugate Chem.* **2010**, *21*, 496 – 504.
[21] a) Y. Liu, Y. Zhong, J. Nan, W. Tian, *Macromolecules* **2010**, *43*, 10221 – 10230; b) Y. Bai, X. Fan, W. Tian, H. Yao, L. Zhuo, H. Zhang, W. Fan, Z. Yang, W. Zhang, *Polymer* **2013**, *54*, 3566 – 3573.

Received: March 10, 2016
Revised: March 29, 2016
Published online on May 11, 2016